Recent progress in avalanche photodiodes for sensing in the IR spectrum

S. J. Maddox,[2] M. Ren,[1] M. E. Woodson,[1] S. R. Bank,[2] and J. C. Campbell[1]

[1] *Department of Electrical and Computer Engineering, University of Virginia, Charlottesville, VA 22904*
[2] *Microelectronics Research Center, The University of Texas, Austin, TX 78758*

Abstract—We report low-noise avalanche gain from photodiodes composed of a previously uncharacterized alloy, $Al_xIn_{1-x}As_ySb_{1-y}$, grown lattice-matched on GaSb substrates. By varying the aluminum content the direct bandgap can be tuned from 0.25 eV (0% aluminum) to 1.24 eV (75% aluminum), corresponding to photon wavelengths from 5000 nm to 1000 nm, with the transition from direct-gap to indirect-gap occurring at ~1.18 eV (~72% aluminum), or 1050 nm. This has been used to fabricate separate absorption, charge, and multiplication (SACM) APDs using $Al_{0.7}In_{0.3}As_{0.3}Sb_{0.7}$ for the multiplication region and $Al_{0.4}In_{0.6}As_{0.3}Sb_{0.7}$ for the absorber. Gain values as high as 100 have been achieved and the excess noise factor is characterized by a k value of 0.01, which is comparable to or below that of Si. In addition, since the bandgap of the absorption region is direct, its absorption depth is 5 to 10 times shorter than indirect-bandgap silicon, potentially enabling significantly higher operating bandwidths.

Keywords: avalanche photodiodes, infrared detectors, photodiodes

1. INTRODUCTION

Over the past five decades, avalanche photodiodes (APDs) have been utilized for a wide range of commercial, military, and research applications. From the mid 1970's to the present, optical communications,[1] imaging,[2,3] and single photon detection[4,5] were the primary driving forces for research and development of APDs. Relative to PIN photodiodes, the internal gain of APDs provides higher receiver sensitivity and dynamic range with concomitant increases in loss margins.[6-10] Two figures of merit for APD optical receivers are the excess noise factor and the gain-bandwidth product. Both are linked to the k factor, which is the ratio of the electron, α, and hole, β, ionization coefficients. The mean-squared shot-noise current can be expressed as[2] $\langle i_{shot}^2 \rangle = 2q(I_{ph}+I_{dark})M^2F(M)\Delta f$ where I_{ph} and I_{dark} are the primary photocurrent and dark current, respectively, M is the avalanche gain, Δf is the bandwidth, and $F(M)$ is the excess noise factor. In the local field model[11] the excess noise factor is given by $F(M) = kM+(1-k)[2-1/M]$. The excess noise factor increases with increasing gain but increases more slowly the lower the value of k. It follows that higher receiver sensitivities are achieved with low k values. The first high-performance APDs for short-wavelength infrared (SWIR) were separate absorption, charge, and multiplication (SACM) APDs that incorporated InP multiplication regions and lattice-matched $In_{0.53}Ga_{0.47}As$ (referred to in the following as InGaAs) absorption layers. These APDs achieved good receiver sensitivity up to bit rates of 10 Gb/s InP/InGaAs.[12-14] However, the relatively high k value of InP, k ~ 0.5, resulted in high excess noise. Recently, M. Nada et al., have reported receiver sensitivity of – 21 dBm at 25 Gb/s and 10^{-12} bit error rate using AlInAs/InGaAs APDs, in which the k value is ~ 0.2.[15] However, for the past 30 years, the "champion" material candidate for high performance APDs is Si, which has measured k values ~ 0.02.[16,17] Unfortunately, as is well known, the bandgap of Si obviates operation at wavelengths > 1.0 μm. There have been numerous research efforts to achieve the excellent avalanche gain characteristics of Si in the SWIR. One approach has been to combine a Ge absorption region with a Si multiplication layer in an SACM APD.[18-20] These APDs have achieved comparable to the best III-V compound APDs but not superior, as would have been expected owing to their low k value. The reason is that their high dark current, which arises from the lattice mismatch between Ge and Si, contributes enough to the noise to offset the lower excess noise factor.

In this paper we report SACM avalanche photodiodes fabricated from $Al_xIn_{1-x}As_ySb_{1-y}$, grown on GaSb. The excess noise factor of the $Al_{0.7}In_{0.3}As_{0.3}Sb_{0.7}$ multiplication region is characterized by a k value of 0.01, which is comparable to, or below, that of Si. Further, the lattice-matched $Al_{0.4}In_{0.6}As_{0.3}Sb_{0.7}$ absorbing region extends the operating wavelength beyond 1600 nm and offers gains > 100. These APDs combine the excellent gain/noise characteristics of Si with the low dark current and high speed of the III-V compound APDs.

Image Sensing Technologies: Materials, Devices, Systems, and Applications III, edited by Nibir K. Dhar, Achyut K. Dutta, Proc. of SPIE Vol. 9854, 985405 · © 2016 SPIE · CCC code: 0277-786X/16/$18 · doi: 10.1117/12.2229774

2. CRYSTAL GROWTH AND DEVICE FABRICATION

The epitaxial layers were grown on n-type Te-doped GaSb (001) substrates by solid-source molecular beam epitaxy (MBE). In order to bypass the wide miscibility gap present in the $Al_xIn_{1-x}As_ySb_{1-y}$ material system, these layers were grown as a digital alloy of the binary alloys AlAs, AlSb, InAs, and InSb, using a digital alloy period of 3 nm and the following layer sequence: AlSb, AlAs, AlSb, InSb, InAs, Sb.[21,22] The bandgap can be tuned by changing the Al

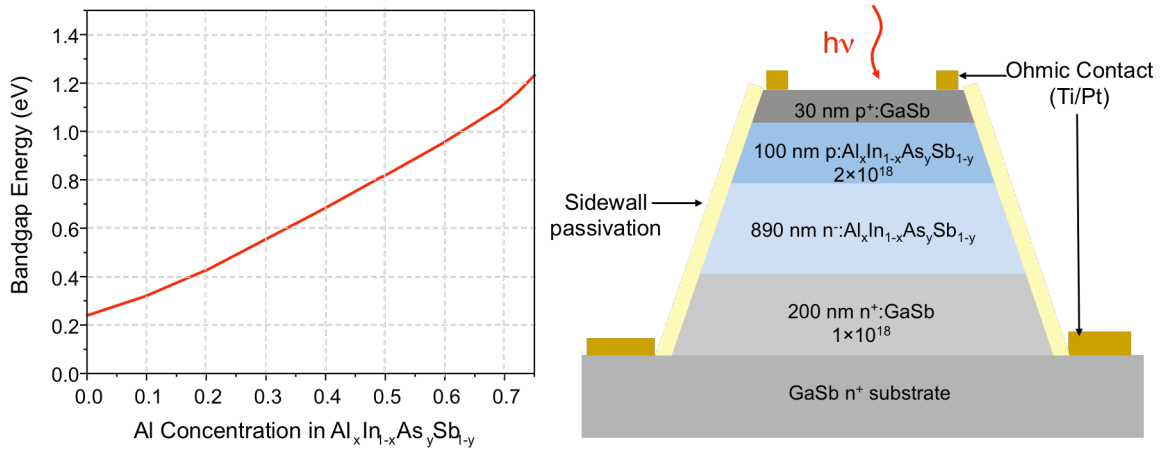

(a) (b)

Figure 1. (a) Schematic cross section of $Al_xIn_{1-x}As_ySb_{1-y}$ homojunction APD and (b) bandgap energy versus Al concentration.

concentration, as shown in Fig. 1(a).[22] Initial studies of the photodiode characteristics were carried out on $Al_xIn_{1-x}As_ySb_{1-y}$ homojunction devices in which the Al concentration was varied from 0.3 to 0.7. Figure 1 (b) shows a schematic cross section of the homojunction structure. For the SACM structure, $Al_{0.4}In_{0.6}As_{0.6}Sb_{0.6}$ and $Al_{0.7}In_{0.3}As_{0.3}Sb_{0.7}$ layers were used for the absorption and multiplication regions, respectively. A schematic cross section and the electric field profile of the $Al_xIn_{1-x}As_ySb_{1-y}$ SACM APD are shown in Figure 2. The structure includes a top GaSb contact layer. Beneath the p-type contact layer is a p^+:$Al_{0.7}In_{0.3}As_{0.3}Sb_{0.7}$ (2×10^{18}cm^{-3}, 100 nm) blocking layer. The p^-: $Al_{0.4}In_{0.6}As_{0.6}Sb_{0.4}$ (1,000 nm) absorbing layer is sandwiched between two 100 nm-thick p^+:Al_xIn_{1-}

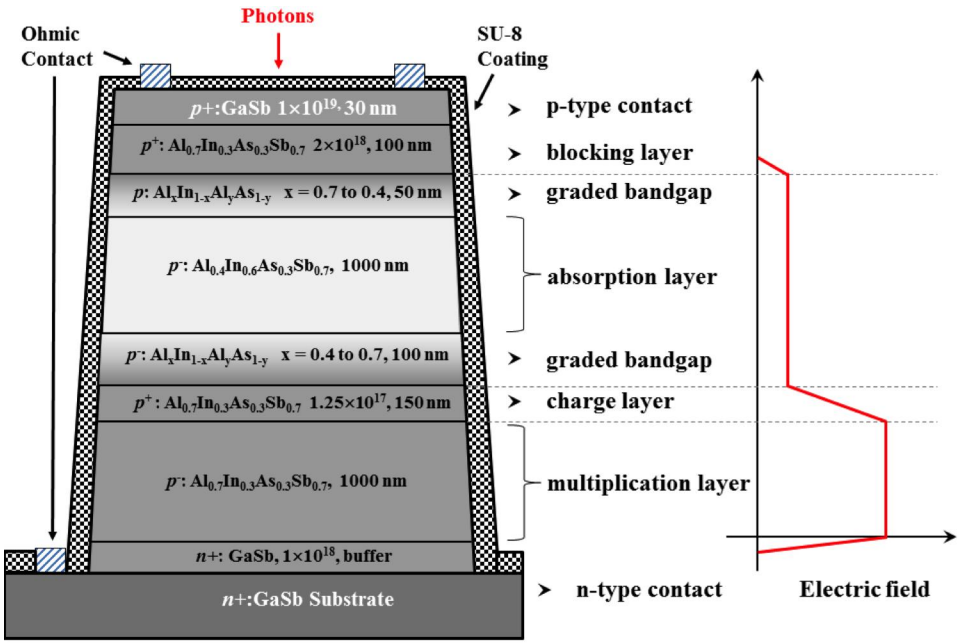

Figure 2. Schematic cross section and electric field profile of $Al_xIn_{1-x}As_ySb_{1-y}$ SACM APD.

$_xAs_ySb_{1-y}$ regions in which the Al composition is graded between x = 0.4 and 0.7. Beneath the absorbing region is a p^+:$Al_{0.7}In_{0.3}As_{0.3}Sb_{0.7}$ (1.25×10^{17} cm^{-3}, 150 nm) charge layer, the p^-: $Al_{0.7}In_{0.3}As_{0.3}Sb_{0.7}$ (1000 nm) multiplication layer, and an n^+: GaSb, $1\sim9\times10^{17}$ n-type contact layer. When reverse biased, a high electric field is formed in the multiplication layer to enable impact ionization. The function of the charge layer is to create a high-low electric filed profile. This enables significant impact ionization in the multiplication region while keeping the field in the absorber low enough to avoid high dark current due to tunneling.

Circular mesas were defined by using standard photolithography and N2/Cl2 inductive coupled plasma (ICP) dry etching. Etching was terminated with a surface-smoothing treatment of bromine methanol. In order to improve passivation and thus reduce the surface leakage current, an SU-8 coating was spun on immediately after the surface treatment. Titanium/gold contacts were deposited by e-beam evaporation onto the mesa and the substrate.

3. PERFORMANCE AND ANALYSIS

By changing the Al concentration from x = 0.7 to 0.3 the optical cutoff can be tuned from ~ 1.0 µm to > 1.6 µm. This is illustrated by the external quantum efficiency measurements on homojunction p-i-n photodiodes with different Al concentration shown in Fig. 3. For all these devices, the thickness of the absorbing region was ~ 1 µm and the top p+:GaSb contact layer was removed except underneath the p-type contacts. Note that these photodiodes do not have an anti-reflective coating.

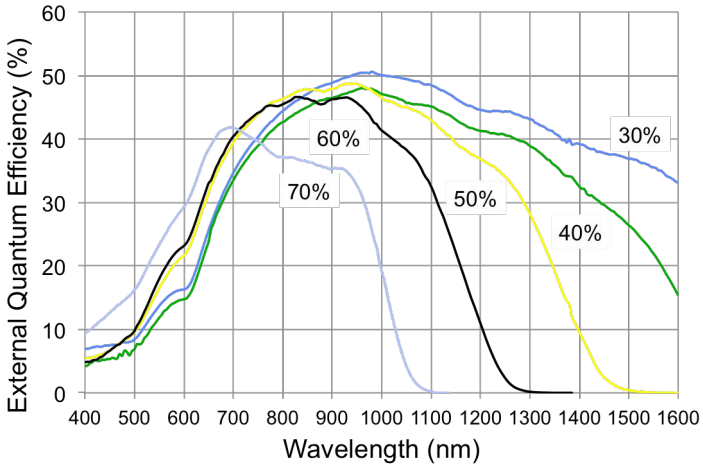

Figure 3. External quantum efficiency versus wavelength of $Al_xIn_{1-x}As_ySb_{1-y}$ p-i-n photodiodes. The Al concentration is noted on each curve.

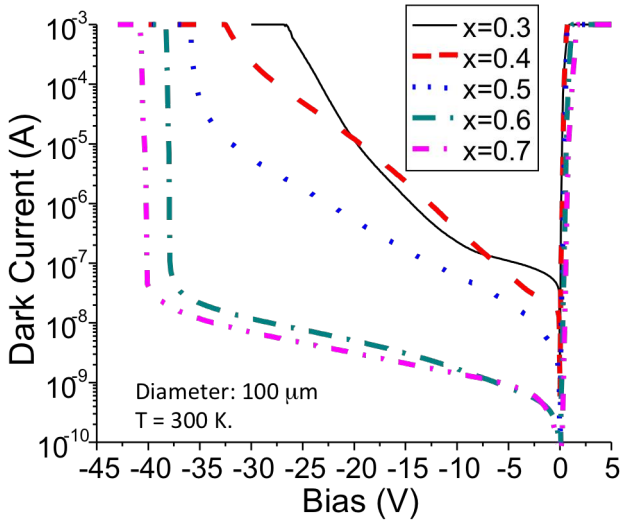

Figure 4. Dark current versus reverse bias for $Al_xIn_{1-x}As_ySb_{1-y}$ p-i-n photodiodes with Al content from 0.3 to 0.7.

Figure 4 shows the dark current versus bias voltage for 100 µm-diameter homojunction devices. The 70% and 60% devices exhibit low dark current and good breakdown characteristics. Tunneling appears to be the dominant mechanism in the 40% and 30% devices. This illustrates the necessity for using an SACM structure in which the high field is confined to a wide bandgap 70% or 60% layer while absorption occurs in lower Al concentration layers with low applied field. For the $Al_{0.7}In_{0.3}As_{0.3}Sb_{0.7}$ device, breakdown occurred at 41 V reverse bias, corresponding to a peak electric field of ~530 kV/cm. The maximum stable gain reached before breakdown was 95. The dark current was ~ 10 nA ($1.5x10^{-3}A/cm^2$) at 90% of breakdown. Total leakage current, I_D, can be expressed as: $I_D = I_{DS} + M I_{DB}$, where I_{DB} *is* the multiplied dark current and I_{DS} is the surface leakage current.

Measurements of dark current versus gain yield I_{DS} ~ 6 nA and I_{DB} ~ 0.14 nA. These measurements indicate that leakage is surface dominated, but further study of passivation techniques promise to push toward buk leakage, further decreasing dark current values.

The dark current, photocurrent, and gain versus bias voltage of the $Al_{0.4}In_{0.6}As_{0.6}Sb_{0.6}/Al_{0.7}In_{0.3}As_{0.3}Sb_{0.7}$ SACM APD shown in Fig. 2 are plotted in Fig. 5. The mesa diameter is 50 µm. The dark current at 95% breakdown is ~ 350 nA, which is approximately 100x lower than that of Ge on Si APDs[18-20] and comparable to that of AlInAs/InGaAs APDs.[15,23] The step in the photocurrent near – 38 V occurs when the edge of the depletion region reaches the absorbing layer, which is referred as punch-through. The gain is plotted on the right vertical axis. Gain values as high

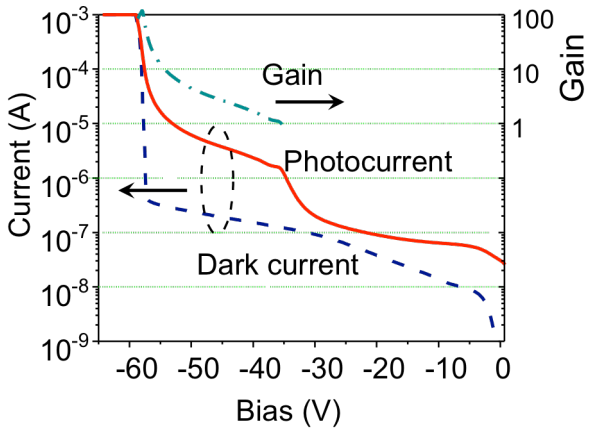

Figure 5. Dark current, photocurrent, and gain versus excess bias for a 50 µm-diameter $Al_{0.4}In_{0.6}As_{0.6}Sb_{0.6}/Al_{0.7}In_{0.3}As_{0.3}Sb_{0.7}$ SACM APD.

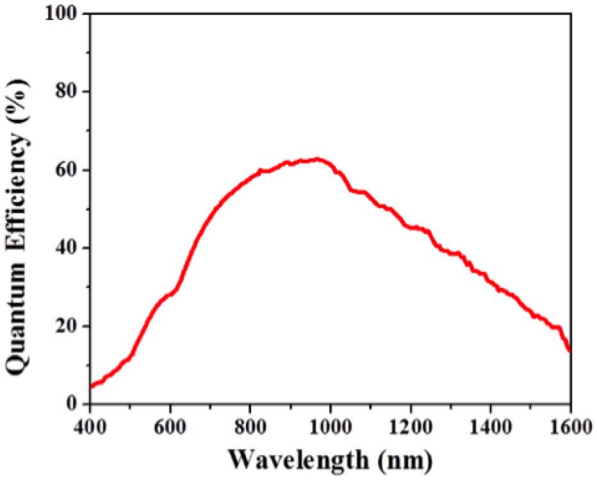

Figure 6. External quantum efficiency versus wavelength of $Al_xIn_{1-x}As_ySb_{1-y}$ SACM APD.

as 100 have been observed. Due to the high field in the multiplication layer, there is some impact ionization at punch-through. By fitting the excess noise using the algorithm reported by H.-D. Liu et al.[24] the gain at punch-through was estimated as M = 1.2. This was confirmed by comparing the photoresponse with an $Al_{0.4}In_{0.6}As_{0.6}Sb_{0.6}$ p-i-n photodiode that has the same 1000 nm absorption layer. The normalized external quantum efficiency was measured at -38 V bias using a tungsten-halogen light source, a spectrometer, and a lock-in amplifier. As shown in Figure 6, the optical cutoff wavelength goes beyond 1.6 µm. Note that the absorption layer is only 1,000 nm thick. Higher quantum

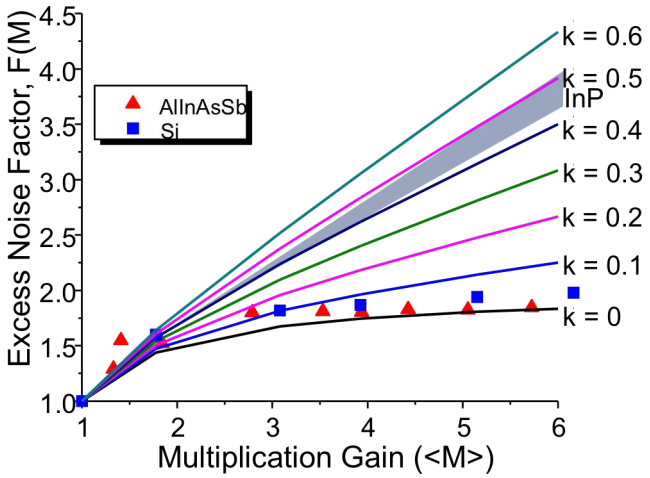

Figure 7. Figure 5. Measured excess noise factor versus gain for multiplication $Al_xIn_{1-x}As_ySb_{1-y}$ SACM APD (■) and a Si APD (▲). The solid lines are plots of the excess noise factor using the local field model for k values from 0 to 0.6. Both the Si and $Al_xIn_{1-x}As_ySb_{1-y}$ SACM APD are characterized by a k value of ~ 0.015. The shaded region for k ≥ 0.45 denotes typical values for APDs that employ InP multiplication regions.

efficiency, particularly at longer wavelengths, can be achieved with thicker $Al_{0.4}In_{0.6}As_{0.6}Sb_{0.4}$ absorption layers and by using an anti-reflection coating on the top surface. Figure 7 shows the excess noise figure versus multiplication gain, for both the $Al_xIn_{1-x}As_ySb_{1-y}$ SACM APD (■) and a Si APD (▲) measured by an HP 8970 noise figure meter. The solid lines are plots of the excess noise for k-values from 0 to 0.6 using the local-field model.[11] The shaded region for $k \geq 0.45$ denotes typical values for APDs that employ InP multiplication regions. The measured $Al_xIn_{1-x}As_ySb_{1-y}$ SACM APD excess noise corresponds to an estimated *k*-value of 0.01. This is the lowest noise reported for an APD operating in the visible or short-wave infrared. Given the relatively thick multiplication regions of the APDs reported here, we suggest that the measured *k* values reflect the bulk ionization characteristics of $Al_{0.7}In_{0.3}As_{0.3}Sb_{0.7}$. Low *k* factor values have been observed for detectors fabricated from its constituent materials InAs[25,26] and InSb.[27] Those materials are characterized by very low electron masses, large hole masses, and large separation between the Γ conduction band minimum and the X and L satellite valleys. The scattering rates for impact ionization tend to be higher than phonon scattering to the satellite valleys. Additionally, previous studies have shown that the addition of Al to a material does not significantly increase its *k*-value, as with AlAsSb[28] and InAlAs.[23] Furthermore, initial Monte Carlo studies indicate that a high hole scattering rate may contribute further to the low *k*-value.

4. SUMMARY

We report SACM avalanche photodiodes fabricated from $Al_xIn_{1-x}As_ySb_{1-y}$, grown on GaSb. The excess noise factor of the $Al_{0.7}In_{0.3}As_{0.3}Sb_{0.7}$ multiplication region is characterized by a k value of 0.01, which is comparable to or below that of Si and gains >100. Further, the lattice-matched $Al_{0.4}In_{0.6}As_{0.3}Sb_{0.7}$ absorbing region extends the operating wavelength beyond 1600 nm. These APDs combine the excellent gain/noise characteristics of Si with the low dark current and high speed of the III-V compound APDs.

5. REFERENCES

1. J. C. Campbell, "Advances in photodetectors," in Optical Fiber Telecommunications, Vol. 5, Part A: Components and Subsystems, 5th Edition, I. Kaminow, Tingye Li, and A. E. Wilner, editors, Academic Press, February 22, 2008.
2. N. Bertone and W. R. Clark, "APD ARRAYS - Avalanche photodiode arrays provide versatility in ultrasensitive applications," Laser Focus World, vol. 43, no. 9, pp. 69-73, Sept. 2007.
3. P. Mitra, J. D. Beck, M. R. Skokan, J. E. Robinson, J. Antoszewski, K. J. Winchester, A. J. Keating, T. Nguyen, K. K. M. Silva, C. A. Musca, J. M. Dell, and L. Farone, "Adaptive focal plane array (AFPA) technologies for integrated infrared microsystems," vol. 6232, p 62320G-1-11, 2006.
4. A. Tosi, N. Calandri, M. Sanzaro, and F. Acerbi, "Low-noise, low-jitter, high detection efficiency InGaAs/InP single-photon avalanche diode," IEEE J. Sel. Top. Quantum Electron., vol. 20, no. 6, p 3803406 (6 pp.), Nov.-Dec. 2014.
5. X. Jiang, M. Itzler, K. O'Donnell, M. Entwistle, M. Owens, K. Slomkowski, and S. Rangwala, "InP-Based Single-Photon Detectors and Geiger-Mode APD Arrays for Quantum Communications Applications," IEEE J. Sel. Top. Quantum Electron., vol. 21, no. 3, p 3800112 (12 pp.), May-June 2015.
6. S. D. Personick, "Receiver design for digital fiber-optic communication systems, Parts I and II," Bell Syst. Tech. J., vol. 52, pp. 843-886, 1973.
7. R. G. Smith and S. D. Personick, "Receiver design for optical fiber communications systems," in Semiconductor Devices for Optical Communication. New York: Springer-Verlag, 1980, ch.4.
8. S. R. Forrest, "Sensitivity of avalanche photodetector receivers for high-bit-rate long-wavelength optical communication systems," in Semiconductors and Semimetals, vol. 22: Lightwave Communications Technology. Orlando, FL: Academic Press, 1985, Ch. 4.
9. B.L. Kasper and J.C. Campbell, "Multigigabit-per-Second Avalanche Photodiode Lightwave Receivers," J. Lightwave Tech., vol. LT-5, pp. 1351 (1987).
10. J. C. Campbell, "Recent advances in avalanche photodiodes," J. Lightwave Tech.. vol. 34, no. 2, pp. 278-285, 2016.
11. McIntyre, R. J., "Multiplication noise in uniform avalanche diodes," IEEE Trans. Electron Dev. , vol. ED-13, pp. 154-158, 1966.
12. C. Y. Park, K. S. Hyun, S. K. Kang, M. K. Song, T. Y. Yoon, H. M. Kim, H. M. Park, S.-C. Park, Y. H. Lee, C. Lee, and J. B. Yoo, "High-performance InGaAs/InP photodiode for 2.5 Gb/s optical receiver," Optical and Quantum Elect., vol. 24, no. 5, pp. 553-559, 1995.
13. Ghulam Hasnain, Wayne G. Bi, S. Song, John T. Anderson, Nick Moll, Chung-yi Su, James N. Hollenhorst, Nicholas D. Baynes, I. Athroll, Sean Amos, and R. M. Ash, "Buried-Mesa Avalanche Photodiodes", IEEE J. Quantum Elect., vol. 34, no. 12, pp. 2321-2326, 1998.

14. M. A. Itzler, C. S. Wang, S. McCoy, N. Codd, N. Komaba, “Planar bulk InP avalanche photodiode design for 2.5 and 10 Gb/s applications,” Proceedings of ECOC '98 - 24th European Conference on Optical Communication, vol.1, pp. 59-60, Madrid, Spain 20-24 Sept. 1998.
15. M. Nada, Y. Muramoto, H. Yokoyama, T. Ishibashi and H. Matsuzaki, “Triple-mesa avalanche photodiode with inverted p-down structure for reliability and stability,” J. Lightwave Tech., vol. 32, no.81, pp. 1543–1548, April 2014.
16. P. P. Webb, R. J. McIntyre, and J. Conradi, “Properties of avalanche photodiodes,” *RCA Review*, v 35, n 2, p 234-78, Jan. 1974.
17. V. M. Robbins, T. Wang, K. F. Brennan, K. Hess, and G. E. Stillman, “Electron and hole impact ionization coefficients in (100) and in (111) Si,”Journal of Applied Physics, vol. 58, no. 12, pp. 4614-4617, 15 Dec. 1985.
18. Y. Kang, M. Zadka, S. Litski, G. Sarid, M. Morse, and M. J. Paniccia, Y. -H. Kuo, J. Bowers, A. Beling, H. –D. Liu, J. Campbell and A. Pauchard, “Epitaxially-grown Ge/Si avalanche photodiodes for 1.3 μm light detection,” Nature Photonics, vol. 3, pp. 59-63, January 2009.
19. Y. Kang, Z. Huang, Y. Saado, J. C. Campbell, A. Pauchard, J. E. Bowers, and M. J. Paniccia, “High performance Ge/Si avalanche photodiodes development in Intel,” 2011 Conference on Optical Fiber Communication - OFC 2011 Collocated National Fiber Optic Engineers Conference OFC/NFOEC 2011, p 3 , 2011.
20. N. Duan, T. Liow, A. Lim, L. Ding, and G. Q. Lo, “310 GHz gain-bandwidth product Ge/Si avalanche photodetector for 1550 nm light detection,” Opt. Express, vol. 20, pp. 11031-11036, 2012.
21. L. G. Vaughn, L. R. Dawson, E. A. Pease, L. F. Lester, H. Xu, Y. Jiang, and A. L. Gray, “Type I mid-infrared MQW lasers using AlInAsSb barriers and InAsSb wells,” Proc. SPIE, vol. 5722, pp. 307–318, 2005.
22. S. J. Maddox and S. R. Bank, “Broadly Tunable AlInAsSb Digital Alloys Grown on GaSb,” J. Cryst. Growth Des. (submitted).
23. C. Lenox, P. Yuan, H. Nie, O. Baklenov, C. Hansing, J. C. Campbell, and B. G. Streetman, “Thin multiplication region InAlAs homojunction avalanche photodiodes,” Appl. Phys. Lett., vol. 73, pp. 783-784, 1998.
24. H. Liu, H. Pan, C. Hu, D. McIntosh, Z. Lu, J. C. Campbell, Y. Kang and M. Morse, “Avalanche photodiode punch-through gain determination through excess noise analysis,” J. Appl. Phys., vol. 106, 064507, 2009.
25. A. R. J. Marshall, C. H. Tan, M. J. Steer, and J. P. R. David, “Extremely low excess noise in InAs electron avalanche photodiodes,” IEEE Photon. Technol. Lett., vol. 21, pp. 866-868, 2009.
26. Wenlu Sun, Zhiwen Lu, Xiaoguang Zheng, J. C. Campbell, S. J. Maddox, H. P. Nair, and S. R. Bank, “High-Gain InAs Avalanche Photodiodes,” IEEE J. Quantum Electronics, vol. 49, no. 2, pp. 154-61, Feb. 2013.
27. J. Avautret, J.P. Perez, A. Evirgen, J. Rothman, A. Cordat, and P. Christol, “Characterization of midwave infrared InSb avalanche photodiode,” J. Appl. Phys., vol. 117, no. 24, p 244502 (6 pp.), 28 June 2015
28. C. H. Tan, S. Xie, J. Xie, “Low noise avalanche photodiodes incorporating a 40 nm AlAsSb avalanche region,” IEEE J. Quant. Electron., vol. 48, pp. 36-41, 2011.